International Journal of Chemical and Biochemical Sciences
(ISSN 2226-9614)

Journal Home page: www.iscientific.org/Journal.html

Recent advances in the use of atomic force microscopy technique for dye-sensitized solar cells characterization

Ho Soonmin

Faculty of Health and Life Sciences, INTI International University, 71800, Putra Nilai, Negeri Sembilan, Malaysia.

Abstract

Atomic force microscopy has been used to study the topography of the prepared samples. It was noted that the cantilever design has been improved from time to time so that this technique could be used in different environments. Dye-sensitized solar cells have been developed due to their cost-efficiency, environmental friendliness, and lightweight nature. In general, this type of solar cell consists of a few parts, including a sensitizer, photoanode, electrolytes, and counter electrode. Experimental results show that TiO_2, ZnO, Er_2O_3 and indium oxide have been synthesized as photoanodes. The surface roughness, thickness, and grain size of these samples were strongly dependent on experimental conditions. The designed solar cells demonstrate good photovoltaic properties as well.

Keywords: photovoltaic, energy efficiency, energy consumption, semiconductor, dye-sensitized solar cells.

*Corresponding Author, e-mail: soonmin.ho@newinti.edu.my

1. Introduction

Atomic force microscopy was built in 1989 due to the high demand for micro- and nanotechnologies. It could be used to study the properties of the prepared samples from different areas such as biophysics, life science, biological molecules, electrochemistry, material science, and nanotechnology at the nanoscale [1]. It was noticed that the cantilever design has been improved from time to time so that this technique could be utilized in different environments [2]. Silicon and silicon nitride were used to produce cantilevers. The length, width, and thickness were found to be 40 µm-500 µm, 50 µm, and 0.5 µm-8 µm, respectively. In general, the interaction between the surface of the sample and a sharp probe could be measured through the scanning process [3]. As a result, surface height data, roughness, structural topography, and mechanical stiffness will be reported via high-resolution three-dimensional images (Table 1). AFM images could be captured under different conditions, including vacuum, air, and aqueous. In terms of sample preparation, it was relatively simple (compared to the TEM technique), and little-to-no damage could be observed [4]. In addition, the freezing process is not required, which is good for biological systems [5]. Technically speaking, several types of applied forces (Table 2) have been highlighted in atomic force microscopy operations. The selection of these modes chiefly depends on the properties of the prepared sample, which must be tested [6]. In contact mode (figure 1), the tip contacted the surface of the sample, and the resultant force was repulsive [7]. While the tip was found to never contact the surface of the sample in noncontact mode, and the resultant force was attractive. On the other hand, attractive or repulsive force could be seen in the tapping mode due to the tip being shifted toward or away from the surface of the samples. The net force is found to be attractive, then becomes a repulsive force in the force mode because the sample is moved towards the tip. Several disadvantages could be seen with this technique. For example, very slow imaging speed [8], more complicated operation procedures, especially for biological samples, and light color cannot be scanned properly. In many cases, the AFM technique has been utilized for nanoscale characterization in polymer sciences [9]. Optical microscopy and Fourier transform infrared spectroscopy were considered popular techniques to investigate the behaviors of polymer; they showed some disadvantages, such as a diffraction limit and very low resolution, respectively. The AFM technique offered important information such as lamellar reorganizations, crystal growth, spherulites, and crystal melting [10]. On the other hand, the AFM technique could be used to study single biomolecules [11] because it can scan the surface of samples in liquid conditions (nanometer resolution conditions). Water-soluble properties and membrane proteins can be measured easily due to their excellent signal-to-noise ratio and high-resolution [12]. This technique provided some results, such as elasticity, height of proteins, 3-dimensional structure formation [13], molecular volumes of proteins, ligand-receptor interaction, and proteomics. It was noted that AFM technology has been employed in regenerative

medicine and tissue engineering [14] as well. In this work, the topography of the obtained photoanode was studied using atomic force microscopy technique. Thickness, surface roughness and the grain size could be investigated using this technique. Photovoltaic properties of the prepared materials have been highlighted also.

2. Dye-sensitized solar cells

Solar energy has been developed in many countries. Several advantages have been highlighted, such as renewable energy sources [15], low maintenance costs [16], clean energy [17] and the ability to reduce electricity bills [18]. Solar energy can replace fossil fuels to generate electricity without releasing greenhouse gases into the environment [19]. In general, solar panels can be installed on buildings to heat water and power homes as well [20]. Dye-sensitized solar cells were developed in 1991 for several reasons, such as cost-efficiency [21], environmental friendliness [22], lightweight [23], and simple fabrication behaviors [24]. In general, this type of solar cell consisted of a few parts, including a sensitizer, photoanode, electrolytes, and counter electrode [25]. At present, researchers have reported that the most popular conditions were TiO_2 (as phot anode electrode), N719 ruthenium-based dyes, platinum (counter electrode), and I_3^-/I^- (as redox electrolyte). During the experiment, the photoanode, counter electrode, and redox electrolyte were responsible for light absorption, the redox pair reduction process, and dye reduction, respectively [26]. In terms of mechanism, the light moved via electrode, was absorbed by dye [27], and finally reached the excited state. Following that, these electrons will be transferred to the conduction band (semiconductor materials), and eventually shifted to the external circuit [28]. At the end of the process, oxidized dye will be reduced (counter electrode) to complete the circle. The main challenges in the DSSC were the corrosive electrolyte [29] and the expensive counter electrode (platinum). However, these issues have been solved, such as using conducting polymers as counter electrode and polyelectrolyte to replace liquid electrolyte [30]. Lai and co-workers [31] have reported that higher conversion efficiency (Table 3) in DSSC with TiO_2 strip compared to without TiO_2 strip, due to the one-dimensional protrusive structure, successfully enhanced surface area in the solar cells. During the experiment, TiO_2 strips (height=90 nm, length=5 mm, linewidth=15 μm, period=60 μm) were synthesized via the physical vapor deposition method and the photolithography technique. Following that, a TiO_2 strip was deposited on the TiO_2 compact layer (thickness=22 nm, substrates= fluorine doped tin oxide glass) as shown in AFM images (figure 2). Rs, Rct and Rec were defined as series resistances related to electron transport at the FTO/photoelectrode interface, electrolyte/Pt layer interface, and photoelectrode/electrolyte interface, respectively. It was noted that the Rs value was smaller in TiO_2 strip samples because electrons were successfully transported from the solar cell to the external circuit. When the electron injection was more efficient from the dye solution to the conduction band (photoelectrode), larger Rrec values could be observed in TiO_2 strip cells. When a smaller probability occurred in the recombination process (holes and electrons), it caused higher average electron lifetimes in these samples.

Titanium dioxide has been used in dye-sensitized solar cells (DSSC) due to its low-cost, non-toxicity, and unique properties. The obtained band gap was 3.2 eV, electrons can jump to the conduction band under ultraviolet conditions. Following that, electron-hole pairs will be generated. Photoanode and photocathode fabrication have been demonstrated by Leonardo and co-workers [32] and co-workers. Deposition of TiO_2 onto FTO glass through a spin coater (speed=1000 rpm, time=10 s). While platinum has been selected as a counter electrode due to its efficiency. The drop casting technique was employed to produce photocathode by using a hexachloroplatinic acid solution. The topography of the obtained samples was studied using the AFM technique. A smaller surface roughness value (figure 3) could be seen in the TiO_2 photoelectrode (65 μm) if compared to platinum (23 nm). Also, a completely homogeneous surface was detected (TiO_2 photoelectrode) to reach higher efficiency in DSSC devices. Based on the obtained results, it was proven that the highest efficiency was observed (Table 4) when the natural dye was Alstroemeria flower dyes (1.74%) because of the presence of cyanidin-3-glycosides. The compact titanium dioxide has been deposited onto FTO substrates [43] using the radio frequency reactive magnetron sputtering method (sputtering pressure=10 mtorr, substrate temperature=300 °C, rf power=100W, distance between target and substrate=80 mm). The prepared samples showed good adherence and no cracking. It was noticed that the deposition rate decreased when the oxygen partial pressure was increased. In addition, sputtering voltage drops as the oxygen flow rate increases during the deposition process. AFM images (figure 4) highlighted columnar structures in the prepared samples. However, a rougher surface could be seen in number 8 samples (1.21 nm) than number 2 sample (0.33 nm), indicating a larger surface area and greater photocatalytic activity. The number 2 sample was synthesized in an oxygen and argon atmosphere, while the number 8 was produced in the presence of nitrogen gas. In terms of photovoltaic properties, TiO_2/FTO with carbon electrode has lower power conversion efficiency (1.51%), open circuit voltage (Voc) (0.522 V) and short circuit current density (Jsc) (4.33 mA/cm^2) than platinum counter electrode (4.98 % to 7.65%, 0.622 V to 0.762 V, 12.38 mA/cm^{2}to 13.95 mA/cm^2). Indium oxide films showed weak photo electro activity, causing very poor power conversion efficiency in DSSC devices. Many experiments have been conducted [44] and low current densities such as 0.75 mA/cm^2 and 3.83 mA/cm^2 have been reported. The influence of annealing temperature on the properties of spin-coated thin films was studied [45]. The physical and electrical properties of the prepared films have been investigated (table 5). RMS surface roughness (2 nm, 11 nm, and 29 nm) and thickness (346.1 nm, 591.7 nm, 1.4 μm) increased when the annealing temperature was increased from 350°C, 450 °C and 550 °C, respectively. It was noted that a more homogeneous structure could be seen at higher temperatures (figure 5). It was noticed that the best temperature was 450 °C, because it offered a low recombination effect, a larger diffusion rate, a longer electron lifetime, and the highest power conversion efficiency value. Based on the literature review (table 6), there are many types of photoanodes that have been used as photoanodes in dye sensitized solar cells.

Table 1: Comparison of different types of microscopy methods

Microscopy	Resolution (nm)	Image size (μm)	Frame rate (FPS)	Main modality
Optical microscopy	200	1000	100	2-dimensional image
Scanning electron microscopy (SEM)	10	1000	20	3-dimensional image
Transmission electron microscopy (TEM)	0.2	100	20	2-dimensional projection
Atomic force microscopy (AFM)	3	100	0.1	3-dimensional topography
Scanning Tunneling Microscopy (STM)	0.1	0.5	0.1	3-dimensional density of states

Table 2: Several types of applied forces in the AFM technique.

	Contact mode	Tapping mode	Phase imaging	Nanoindentation	Peak force QNM	KPFM
Information provided	Roughness, topography	Roughness, topography	Qualitative differentiation between materials + clearer edges within single material	Elastic modulus, hardness	Elastic modulus, adhesion	Contact potential of a surface
Static/dynamic mode	Static mode	Dynamic mode	Dynamic mode	Dynamic/static /quasistatic	Dynamic mode	Dynamic mode
Special requirements	Cantilever for static mode	Cantilever for dynamic mode	Cantilever for dynamic mode	Tip harder if compared to sample	broad tips are supportive	Conductive tip, single or dual pass setup

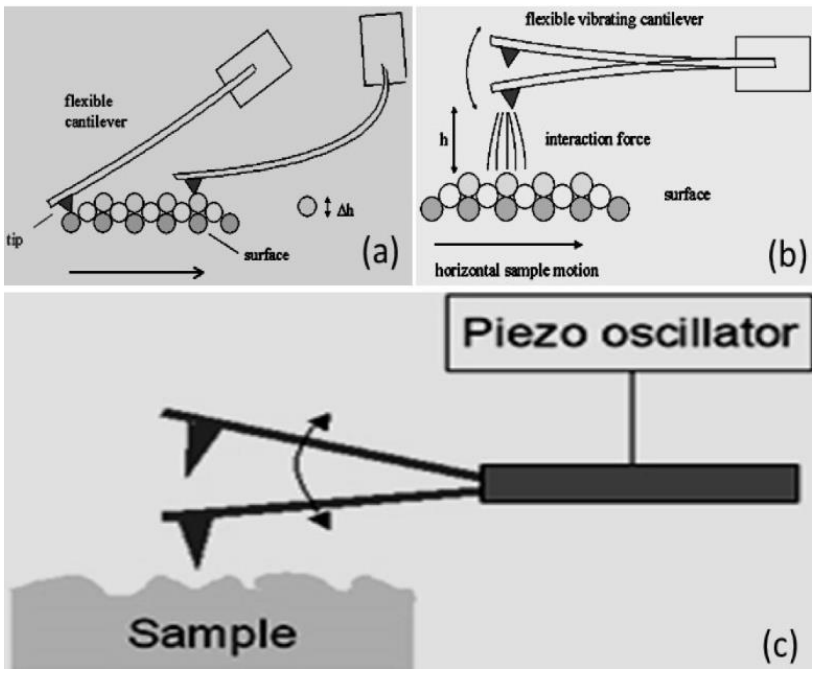

Figure 1: Several types of scanning modes in atomic force microscopy (a) contact mode (b) non-contact mode (c) tapping mode [10]

Table 3: Photovoltaic, resistance, and physical properties of DSSC in different conditions

	Voc (mV)	Isc (mA)	Fill factor (%)	Efficiency (%)	Average electron lifetime (ms)	Average peak frequencies (Hz)	Rs (Ω)	Rct (Ω)	Rec (Ω)
With TiO_2 strip	788	2.26	0.74	4.38	10	15.9	12.3	2.1	20.1
Without the TiO_2 strip	775	1.78	0.7	3.2	7.9	20	17.5	2.6	17.1

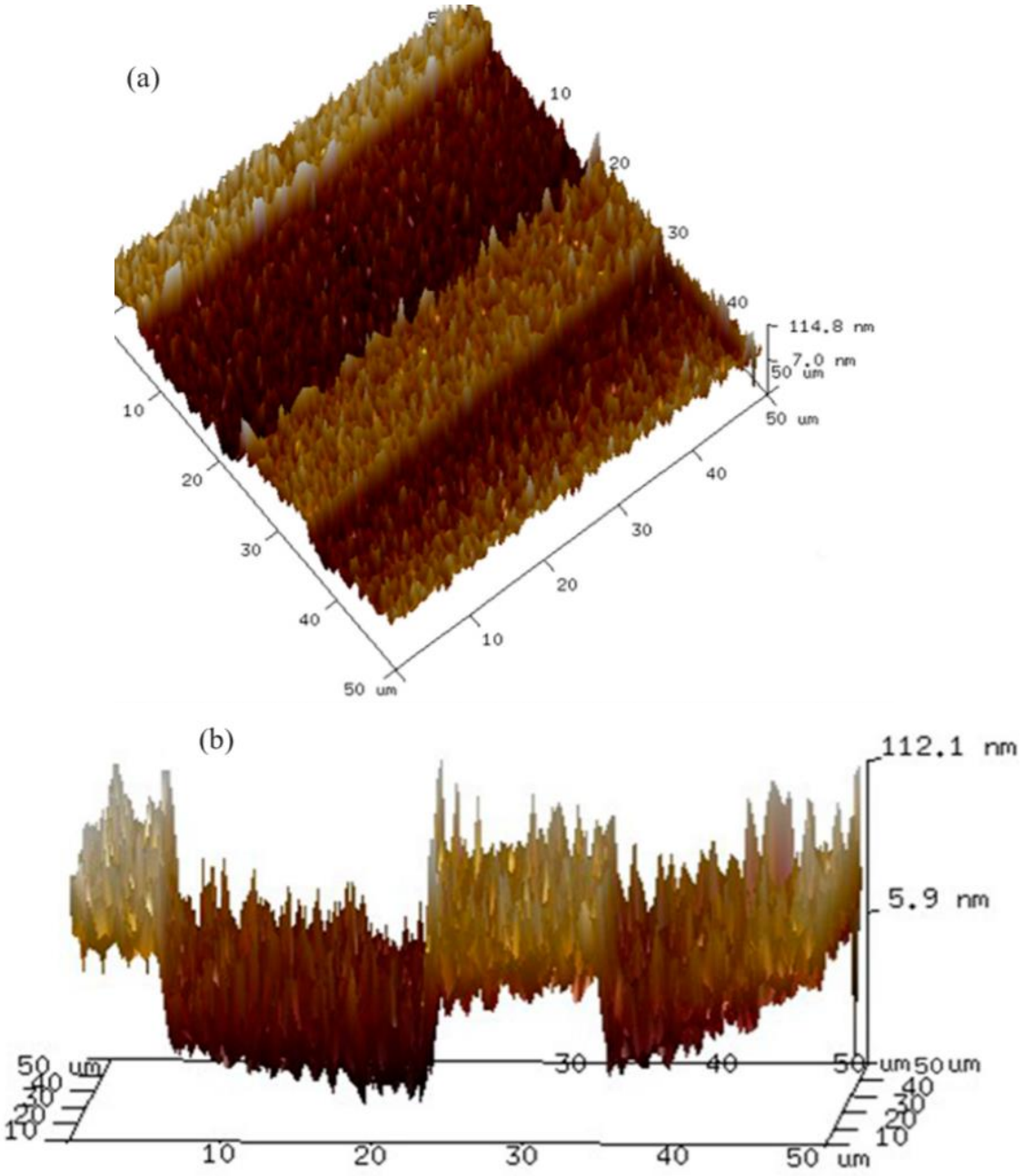

Figure 2:AFM images of TiO_2 strip deposited onto TiO_2 compact layer (a) top view (b) side view [31].

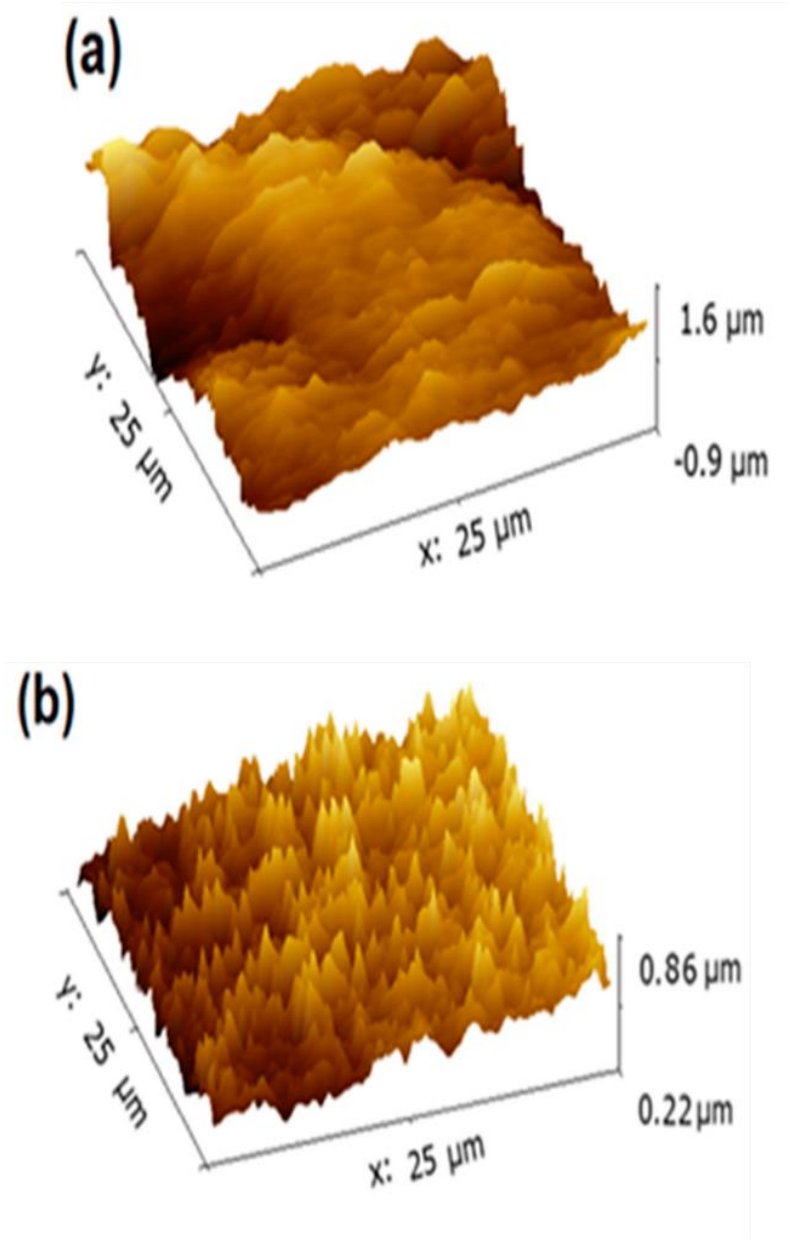

Figure 3: AFM images of (a) TiO_2 and (b) platinum electrode [32]

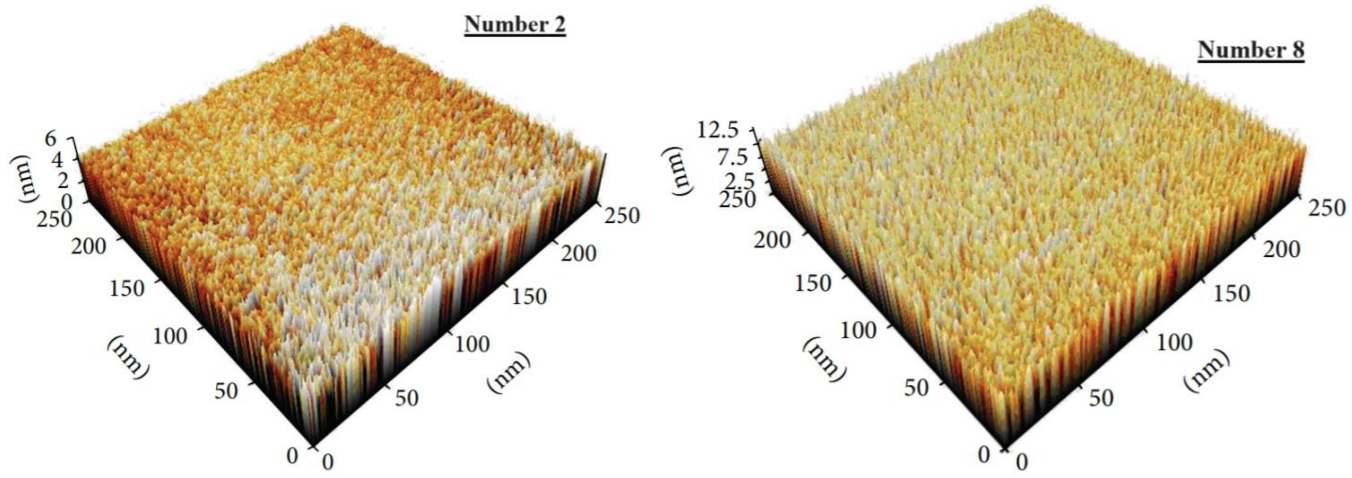

Figure 4: AFM images for number 2 and numbr 8 sample. [43]

Table 4: Photovoltaic properties of DSSC with different natural dyes

Dye	Jsc (mA/cm^2)	Voc (V)	Power conversion efficiency (%)	Researchers
Jabuticaba [33]	0.38	0.41	0.13	Sampaio and co-workers, 2019
Thubergia Erecta [34]	0.27	0.54	0.38	Ferreira and co-workers, 2018
Achiote seeds [35]	1.1	0.57	0.37	Gómez-Ortíz and co-workers, 2010
Henna [36]	0.42	0.54	0.09	Sowmya and co-workers, 2020
Sorghum Stem [37]	1.69	0.34	0.18	Sanda and co-workers, 2021.
Leucanthemum [38]	0.42	0.54	0.88	Ferreira and co-workers, 2020.
Prickly Pear [39]	1.17	0.56	0.56	Purushothamreddy and co-workers, 2020.
Carica Papaya [40]	1.77	0.4	0.29	Ossai and co-workers, 2021.
Chrysanthemum [41]	0.85	0.58	1.35	Leite and co-worker, 2023.
Tropaeolum majus [42]	0.72	0.55	0.28	Singh and co-workers, 2021.

Table 5: Physical, compositional, and electrical properties of the prepared films.

Annealing temperature	350	450	550
Oxygen element (%)	19.37	22.37	27.67
Voc (V)	0.35	0.42	0.36
Particle size (nm) FESEM	52	121	410
Particle size (nm) TEM	62	169	478
Fill factor	0.32	0.43	0.35
Power conversion efficiency (%)	0.28	1.54	0.73
Jsc (mA/cm^2)	2.5	9.2	5.8
crystallite size (nm)	8.381	17.188	19.101
transport resistance (Ω)	215	3.21	198
charge transfer resistance (Ω)	26.2	641	32.12
chemical capacitance (μF)	0.16	6.01	0.52

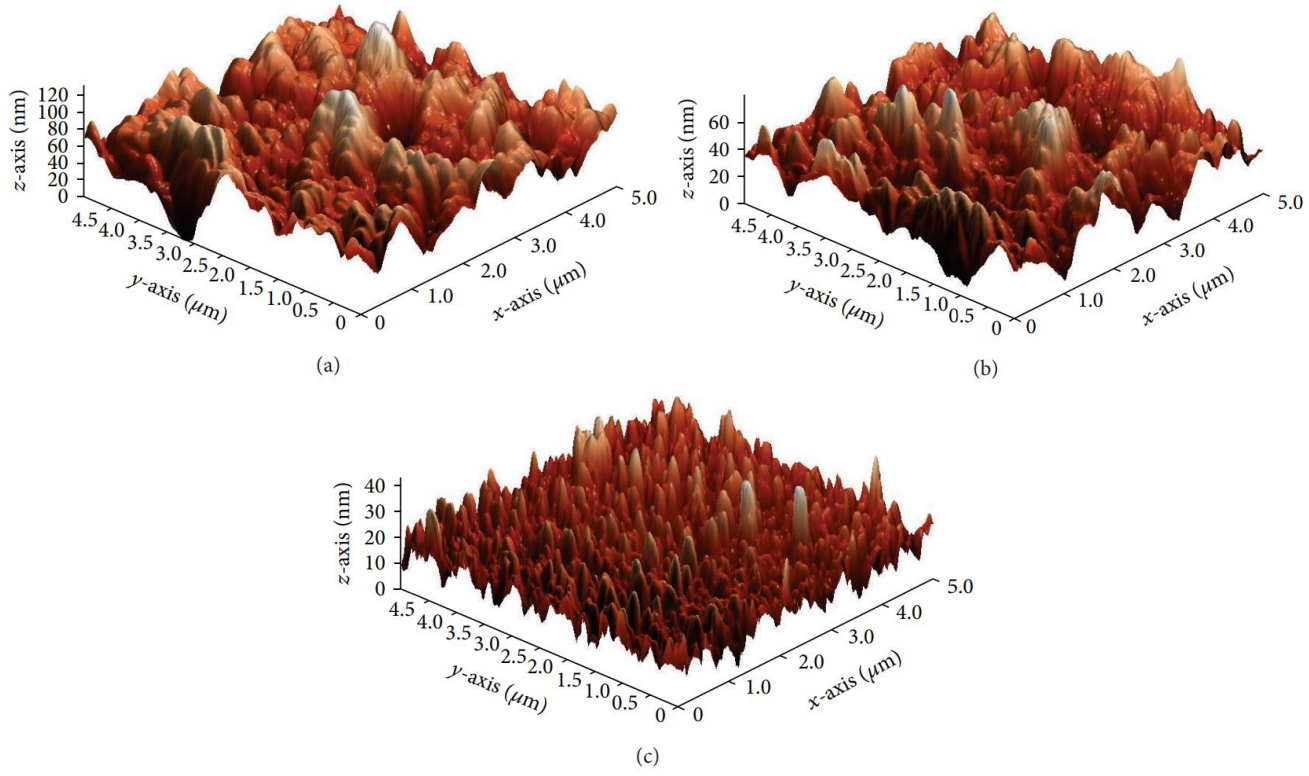

Figure 5: AFM images of In_2O_3 thin films annealed different temperatures such as (a) 350 °C, (b) 450 °C, and (c) 550 °C [45]

Table 6: Various types of materials have been used as photoanode in dye sensitized solar cells.

Materials	Highlighted results
Graphene-TiO_2	Graphene TiO_2 was prepared using spin coating technique [46]. Surface roughness (10.3 nm to 21.1 nm), open circuit voltage (0.699 V to 0.704 V), short circuit current density (19.87 mA/cm^{2}to 19.92 mA/cm^2), and power conversion efficiency (6.32 % to 6.86 %) increased when the graphene content was increased from 0.01% to 1%. The biggest grain size was 38.13 nm when the graphene content was 0.01%.
TiO_2	The sol-gel method has been used to prepare TiO_2 particles using titanium isopropoxide [47]. Particles of different sizes and shapes are uniformly distributed on the surface of the substrates. Obviously, clear porosity could be seen. Higher power conversion efficiency (5.12%), short circuit current density (13.16 mA/cm^2) and open circuit voltage (0.74 V) for N-719 dye (thickness=8.6 μm). Lower power conversion efficiency (4.08 %), short circuit current density (12.18 mA/cm^2) and open circuit voltage (0.675 V) for RK-1 dye (thickness=5.4 μm).
TiO_2	The doctor blade method has been used to prepare TiO_2 particles. AFM images showed a heterogeneous surface with well-ordered morphology [48].
ZnO	ZnO films [49] have been prepared using a hydrothermal process (substrate= FTO, temperature=90 °C) Grain like morphology with a surface roughness of 47 nm. Open circuit voltage and short circuit current were 360 mV and 80 mA, respectively, in the DSSC (Gulmohar flower natural dyes).
ZnO	ZnO-coated TiO_2 (mesoporous structure) was prepared via the spin coating process [50] and successfully enhanced surface roughness. Sharper zinc oxide nanosoars could be observed in AFM images. The highest power conversion efficiency was 7.51%, with an open circuit voltage of 0.66 V, and a short circuit current density of 17.93 mA/cm^2.
ZnO	Undoped zinc oxide films indicated the smallest roughness value with mountain structure [51]. Average particle height increases from 13.9 nm (undoped ZnO layer) to 24.79 nm-28.78nm (aluminium doped ZnO) as reported.
Er_2O_3	Erbium oxide [52] was mixed with TiO_2, deposited onto FTO glass, then heated for 20 minutes at a temperature of 450 °C. Root mean square roughness and average roughness were 68.5 nm and 55.3 nm, respectively. The highest power conversion was 6.39% in 1% Er_2O_3-TiO_2 if compared to 3% Er_2O_3-TiO_2 (5.38%) and 5% Er2O3-TiO2 (5.24%)
NiO	DSSC (rhodamine 6G dye) achieved a power conversion efficiency of 0.973%. The AFM image showed strong vertical order [53] with an average grain size of 16.87 nm.
ZnO	ZnO-Cu_2O films have been synthesized using the photo-irradiation method [54] The average grain size was 36.1 nm, and they reached power conversion efficiency of 10.62%.
TiO_2-CuO	TiO_2-CuO composites have been prepared through the photochemical deposition method [55]. There were different roughness values when the ultraviolet passed hrough titanium dioxide (20.6 nm) and substrate (15.4 nm), when the scanning area was 1μm x 1μm.
Ni-ZnO	Nickel doped zinc oxide has been prepared onto glass using the hydrothermal method [56]. A pillar-like structure could be seen. The growth rate increased when the nickel content was increased.
NiO	There are different results [57] could be seen at lower and higher deposition pressures, such as 0.2 Pa (uniform granular) and 0.4 Pa (needle-like structure).

6. Conclusions

In this work, the atomic force microscopy technique has been used to study the topography of the prepared photoanodes such as titanium oxide, indium oxide, zinc oxide, and erbium oxide. Experimental results confirmed that surface roughness, thickness, and grain size were strongly dependent on the experimental conditions. On the other hand, the power conversion efficacy could be improved when the best conditions have been met.

Acknowledgements:

Author would like to thank to INTI International University, Malaysia for the financial support.

References

[1] O. Qijian, H. Yu and J. Liu. (2022). Application of Atomic Force Microscopy as Advanced Asphalt Testing Technology: A Comprehensive Review. Polymers, https://doi.org/10.3390/polym14142851.

[2] D. Andrius, V. Darius and M. Inga. (2023). Characteristics and Functionality of Cantilevers and Scanners in Atomic Force Microscopy. Materials. https://doi.org/10.3390/ma16196379.

[3] S. Kyriaki, Y. Dido and S. Vasileios. (2023). Atomic Force Microscopy Imaging of Elastin Nanofibers Self-Assembly. Materials. https://doi.org/10.3390/ma16124313.

[4] A. Kassim, S. Nagalingam and S.M. Ho. (2010). XRD and AFM studies of ZnS thin films produced by electrodeposition method. Arabian Journal of Chemistry. 3: 243-249.

[5] T. Misic, V. Petra and C. Andrea. (2023). Insights into the Morphology and Surface Properties of Microalgae at the Nanoscale by Atomic Force Microscopy (AFM): A Review. Water. https://doi.org/10.3390/w15111983.

[6] S. Andreas, G. Colin and A. Eleni. (2019). Atomic force microscopy on biological materials related to pathological conditions. Scanning. https://doi.org/10.1155/2019/8452851.

[7] N. Phuong, N. Sonil and Aymen A. (2020). Recent Applications of Advanced Atomic Force Microscopy in Polymer Science: A Review. Polymers. https://doi.org/10.3390/polym12051142.

[8] X. Fangzhou and Y. Kamal. (2022). Review: Advanced Atomic Force Microscopy Modes for Biomedical Research. Biosensors. https://doi.org/10.3390/bios12121116.

[9] H. Brett and B. Sean. (2018). Feature Tracking for High-Speed AFM Imaging of Biopolymers. International Journal of Molecular Sciences. https://doi.org/10.3390/ijms19041044.

[10] J. Joshi, V. Sarah and E. Andrea. (2022). Atomic Force Microscopy (AFM) on Biopolymers and Hydrogels for Biotechnological Applications—Possibilities and Limits. Polymers. https://doi.org/10.3390/polym14061267.

[11] M. Silvia, A. Pesce and C. Paolo. (2023). Morphological Investigation of Protein Crystals by Atomic Force Microscopy. Crystals. https://doi.org/10.3390/cryst13071149.

[12] O. Tatyana, D. Yuri and S. Natalia. (2018). Atomic Force Microscopy for Protein Detection and Their Physicochemical Characterization. International Journal of Molecular Sciences. https://doi.org/10.3390/ijms19041142.

[13] S. Vasileios, M. Anna and S. Andreas. (2023). Overcoming Challenges and Limitations Regarding the Atomic Force Microscopy Imaging and Mechanical Characterization of Nanofibers.Fibers. https://doi.org/10.3390/fib11100083.

[14] M. Marica, A. Luigi and V. Guarino. (2017). Atomic Force Microscopy: A Powerful Tool to Address Scaffold Design in Tissue Engineering. Journal of Functional Biomaterials. https://doi.org/10.3390/jfb8010007.

[15] Y. Han, Y. Sun and J. Wu. (2023). An efficient and low-cost solar-aided lignite drying power generation system based on cascade utilisation of concentrating and non-concentrating solar energy. Energy. https://doi.org/10.1016/j.energy.2023.129932.

[16] P. Hamed, V. Reza and M. Vahid. (2023). Solar energy status in the world: A comprehensive review. Energy Reports. 10: 3474-3493.

[17] K. Kubilay and I. Dincer. (2023). Green hydrogen production potential of Canada with solar energy. Renewable Energy. https://doi.org/10.1016/j.renene.2023.119766.

[18] A. Bekhouche, A. Kerboub and S.M. Ho. (2023). Improvement of the performance of amorphous silicon solar cells: solar radiation effect. International Journal of Chemical and Biochemical Sciences. 24: 401-405.

[19] R. Yazid, K. Anuar and S.M. Ho. (2011). Preparation and characterization of chemical bath deposited NiSe thin films. Ozean Journal of Applied Sciences. 4: 363-372.

[20] S.M. Ho, C. Edmund and Y. Ahmed. (2018). Advanced research in solar energy: Malaysia, UAE and Nigeria. Eurasian Journal of Analytical Chemistry. 13: 312-331.

[21] K. Sharma, V. Sharma and S. Sharma. (2018). Dye-Sensitized Solar Cells: Fundamentals and Current Status. Nanoscale Research Letters. https://doi.org/10.1186/s11671-018-2760-6.

[22] G. Hajer, M. Frej and A. Ajji. (2023). Flexible PET/(PET-TiO_2) core/shell nanofibrous mats as potential photoanode layer for dye-sensitized solar cells, DSSCs. Materials Chemistry and Physics. https://doi.org/10.1016/j.matchemphys.2023.127911.

[23] G. Aman, S. Maidin and S. Sajjad. (2023). Numerical optimization and performance evaluation of ZnPC:PC70BM based dye-sensitized solar cell. Scientific Reports. DOI: 10.1038/s41598-023-37486-2.

[24] A. Sultan, S. Waseem and M. Reda. (2023). Development of new co-sensitizer based squaraine dyes for enhancing the performance of DSSC. Journal of Molecular Structure. https://doi.org/10.1016/j.molstruc.2023.136130.

[25] K. Said, M. Salah and B. Said. (2023). Effects of chelate ligands containing NN, PN, and PP on the performance of half-sandwich ruthenium metal complexes as sensitizers in dye sensitized solar cells (DSSCs): Quantum chemical investigation. Polyhedron. https://doi.org/10.1016/j.poly.2022.116190.

[26] C. Yigit, O. Mahmut and A. Mert. (2023). DSSCs based on unsymmetrical A_3B type Zn(II) and TiO(IV) naphthalenephthalocyanine/porphyrin cocktail dyes: A potential alternative for ruthenium based sensitizers. Journal of Photochemistry and Photobiology A: Chemistry. https://doi.org/10.1016/j.jphotochem.2023.114642.

[27] C. Rajesh, K. Jae and V. Murali. (2023). Photo-electrodes decorated with carbon quantum dots: Efficient dye-sensitized solar cells. Results in Engineering. https://doi.org/10.1016/j.rineng.2023.101611.

[28] S. Roberto, M. Reina and Z. Pietro. (2023). Laser-induced graphene as a sustainable counter electrode for DSSC enabling flexible self-powered integrated harvesting and storage device for indoor application. Electrochimica Acta. https://doi.org/10.1016/j.electacta.2023.142614.

[29] J. Dix, M. Vyas and M. Manan. (2023). Studies and comparison of natural dye-sensitized solar cells and thin-film solar cells. Materials Today Proceedings. https://doi.org/10.1016/j.matpr.2022.10.222.

[30] K. Inbarajan, S. Sowmya and B. Janarthanan. (2023). Fabrication of dye-sensitized solar cells with the dyeing industrial effluent. Optik. https://doi.org/10.1016/j.ijleo.2023.171471.

[31] W. Lai, T. Lin and X. Lin. (2022). Characteristics of Dye-Sensitized Solar Cells with TiO_2 Stripes. Materials, https://doi.org/10.3390/ma15124212.

[32] R. Leonardo, M. Arcano and D. Cunha. (2023). Evaluation of Solar Conversion Efficiency in Dye-sensitized Solar Cells Using Natural Dyes Extracted from *Alpinia purpurata* and *Alstroemeria* Flower Petals as Novel Photosensitizers. Colorants, 2: 618-631.

[33] D. Sampaio, S. Babu and H. Costa. (2019). Investigation of nanostructured TiO_2 thin film coatings for DSSCs application using natural dye extracted from jabuticaba fruit as photosensitizers. Ionics, 25: 2893–2902.

[34] B. Ferreira, M. Sampaio and S. Babu. (2018). Influence of nanostructured TiO_2 film thickness in dye-sensitized solar cells using naturally extracted dye from *Thunbergia erecta* flowers as a photosensitizer. Optical Materials.86: 39–246.

[35] M. Gómez-Ortíz, A. Vázquez-Maldonado and A. Pérez-Espadas. (2010). Dye-sensitized solar cells with natural dyes extracted from achiote seeds. Solar Energy Materials and Solar Cells. 94: 40–44.

[36] S. Sowmya, P. Prakash and N. Ruba. (2020). A study on the fabrication and characterization of dye-sensitized solar cells with *Amaranthus red* and *Lawsonia inermis* as sensitizers with maximum absorption of visible light. Journal of Materials Science: Materials in Electronics. 31: 6027–6035.

[37] M. Sanda, M. Badu and M. Awudza. (2021). Development of TiO_2-based dye-sensitized solar cells using natural dyes extracted from some plant-based materials. Chemistry International. 7: 9–20.

[38] F. Ferreira, S. Babu, and A. Barros. (2020). Photoelectric performance evaluation of DSSCs using the dye extracted from different color petals of *Leucanthemum vulgare* flowers as novel sensitizers. Spectrochimica Acta Part A: Molecular and Biomolecular Spectroscopy. https://doi.org/10.1016/j.saa.2020.118198.

[39] N. Purushothamreddy, R. Dileep and G. Veerappan. (2020). Prickly pear fruit extract as photosensitizer for dye-sensitized solar cell. Spectrochimica Acta Part A: Molecular and Biomolecular Spectroscopy. https://doi.org/10.1016/j.saa.2019.117686.

[40] A. Ossai, C. Ezike and P. Timtere. (2021). Enhanced photovoltaic performance of dye-sensitized solar cells-based Carica papaya leaf and black cherry fruit co-sensitizers. Chemical Physics Impacts, https://doi.org/10.1016/j.chphi.2021.100024.

[41] A. Leite, H. Cunha and J. Rodrigues. (2023). Construction and characterization of organic photovoltaic cells sensitized by Chrysanthemum based natural dye. Spectrochimica Acta Part A: Molecular and Biomolecular Spectroscopy. https://doi.org/10.1016/j.saa.2022.121780.

[42] S. Singh, C. Maurya and S. Sharma. (2021). Application of new natural dyes extracted from Nasturtium flowers (*Tropaeolum majus*) as photosensitizer in dye-sensitized solar cells. Optik. https://doi.org/10.1016/j.ijleo.2021.167331.

[43] H. Chang, M. Twu and C. Hsu. (2014). Improved Performance for Dye-Sensitized Solar Cells Using a Compact TiO_2 Layer Grown by Sputtering. International Journal of Photoenergy. http://dx.doi.org/10.1155/2014/380120.

[44] R. Sharma, R. Mane and S. Min. (2009). Optimization of growth of In_2O_3 nano-spheres thin films by electrodeposition for dye-sensitized solar cells. Journal of Alloys and Compounds. 479: 840–843.

[45] S. Mahalingam, H. Abdullah and S. Shaari. (2015). Structural, Morphological, and Electron Transport Studies of Annealing Dependent In_2O_3 Dye-Sensitized Solar Cell. The Scientific World Journal. http://dx.doi.org/10.1155/2015/403848.

[46] T. Tsai, S. Chiou and S Chen. (2011). Enhancement of Dye-Sensitized Solar Cells by using GrapheneTiO_2 Composites as Photoelectrochemical Working Electrode. International Journal of Electrochemical Science. 6: 3333-3343.

[47] L. Chougala, S. Yatnatti and R. Kamble. (2017). A Simple Approach on Synthesis of TiO_2 Nanoparticles and its Application in dye Sensitized Solar Cells. Journal of Nano and Electronic Physics. DOI: 10.21272/jnep.9(4).04005.

[48] M. Liang, Y. Fong and C. Khaw. (2014). Studies on the Effects of Crystallite Sizes and Scattering Layers on the Conversion Efficiency of Dye-Sensitized

Solar Cell. Journal of Power and Enerrgy Engineering. 2: 18-24.

[49] L. Joshi, Y. Poudel and L. Mim. (2017). Preparation and Characterization of Zinc Oxide Based Photoanodefor Dye-sensitized Solar Cell using Delonix Regia Natural dye extract. Journal of Nepal Physical Society. 4: 1-6.

[50] K. Susmitha, M. Kumar and G. Rajkumar. (2015). Enhanced dye sensitized solar cell performance with high surface area thin ZnO film and PEDOT:PSS. Solar Energy. 118: 126-133.

[51] A. Aprilia, W. Ode and N. Syakir. (2017). Zinc Oxide/TiO_2 Bilayer Heterojunction as a Working Electrode in Quasi Solid Dye Sensitized Solar Cells. IOP Conf. Series: Materials Science and Engineering 214 (2017) 012033 doi:10.1088/1757-899X/214/1/012033.

[52] A. Ahmad, H. Dafalla and M. Umer. (2021). Enhancing the performance of dye-sensitized solar cell using nano-sized erbium oxide on titanium oxide photoanode by impregnation route. Journal of Photochemistry and Photobiology. https://doi.org/10.1016/j.jpap.2021.100047.

[53] E. Jasim, A. Aboud and M. Rheima. (2022). Nickel oxide nanofibers manufactured via sol-gel method: synthesis, characterization and use it as a photo-anode in the dye sensitized solar cell. Digest Journal of Nanomaterials and Biostructures. 17: 59-64.

[54] A. Nibras, S. Wafaa and H. Dhia. (2020). A comparative study of ZnO, CuO and a binary mixture of ZnO0.5-CuO0.5 with nano-dye on the efficiency of the dye-sensitized solar cell. Journal of Physics: conference Series. doi:10.1088/1742-6596/1664/1/012094.

[55] E. Vigil, A. Lima and E. Pedrero (2008) TiO_2–CuO three-dimensional heterostructure obtained using short time photochemical deposition of copper oxide inside a porous nanocrystalline TiO_2 layer. Microporous and Mesoporous Materials 109 (2008) 560–566.

[56] S. Thakur, J. Kumar and N. Sharma. (2013) Structural and optical study of nickel doped ZnO nanoparticles and thin films for dye sensitized solar cell applications. Journal of Optoelectronics and Advanced Materials, 15: 989-994.

[57] M. Awais, M. Rahman and J. MacElroy. (2010) Deposition and characterization of NiOx coatings by magnetron sputtering for application in dye-sensitized solar cells. Surface and Coatings Technology. 204: 2729-2736.